Progress In Electromagnetics Research Letters, Vol. 104, 169–177, 2022

Abnormal Circularly Polarized Propagation over Terrain Profile with Gaussian Correlated Roughness

Xueyuan Chen, Peng Xu*, Xinguo Ma, Yucheng Yao, and Hui Lv

Abstract—In application to active microwave remote sensing, the counterwise RL (left-hand circularly polarized transmitting and right-hand circularly polarized receiving) and LR polarized bistatic scattering are generally stronger than the likewise LL and RR ones, respectively. In this paper, we investigate the circularly polarized propagation over terrain profile at 1.575 GHz and 900 MHz in application to wireless communication. Completely different from common sense in remote sensing, however, numerical simulations show that field strengths for likewise polarizations are larger than those for counterwise polarizations. For further verification, circularly polarized bistatic scattering from terrain is also provided, which is consistent with previous conclusion that the counterwise LR polarized one is larger. Physical mechanism of such a contradictory behavior is explicated by local Fresnel reflections, and physical insights are offered for terrain propagation of circular polarizations. It is suggested that the likewise configuration be adopted in wireless communication, although the counterwise is adopted in microwave remote sensing.

1. INTRODUCTION

In the past years, circularly polarized waves, due to their good electromagnetic properties, have been extensively studied and applied from aerospace communication equipment [1, 2], RFID systems [3, 4], to remote sensing [5–11]. In radar remote sensing, it was argued that GPS signal scattering from single surface for the likewise polarization yielded 20–30 dB lower level than that for the counterwise one [9, 10], and the scattering strength of likewise circular polarizations can also be comparable to the counterwise one for double-layered surface, where the internal total reflection occurred [11]. On the other hand in wireless communication, predicting the field strength and fading on complex terrain in advance are of significance to construct communication network in terrain efficiently. Wave propagations over irregular terrain were investigated for linear polarizations [12–16]. However, less attention has been paid to circularly polarized propagation over terrain surface. As a result, limited understanding toward the physical insight of circularly polarized propagation behavior is gained from previous research.

In this paper, we report the circularly polarized propagation over composite terrain surfaces with Gaussian roughness at 1.575 GHz and 900 MHz. The numerical Maxwell model is performed by following the procedures in [11] and [17]. Simulated solutions are accelerated by the multilevel UV method [12, 18]. Both field strength at height of 1.8 m above composite terrain profiles and bistatic scattering coefficients are obtained, respectively, in application to wireless communication and remote sensing. Comparisons of wave propagation are made between likewise RR configuration and counterwise LR configuration to examine the dominant field over terrain profile. As a reference, bistatic scattering from the same terrain is also compared between the two configurations.

The composite terrain surface with Gaussian roughness is described in Section 2. In Section 3, the cylindrical incident wave for circular polarization is given and verified, and the formulations of surface

Received 28 April 2022, Accepted 7 June 2022, Scheduled 30 June 2022
* Corresponding author: Peng Xu (xupeng@hbut.edu.cn).
The authors are with the School of Science, Hubei University of Technology, Wuhan 430068, Hubei, China.

integral equation are provided by following numerical solutions by method of moments. The circularly polarized bistatic scattering coefficients and circularly polarized propagation are then computed. In Section 4, the numerical results of circularly polarized propagation and bistatic scattering coefficients are illustrated and compared between the likewise and the counterwise. In Section 5, the physical insights are given about why the dominant circular polarization for propagation is the exact opposite of that for bistatic scattering coefficients. Finally, conclusion is drawn to show which configuration is preferred in application to wireless communication over random terrain surface.

2. MODELING OF COMPOSITE TERRAIN SURFACES WITH GAUSSIAN ROUGHNESS

The Beiseker N15 terrain by the Canada Map Office (CMO) is obtained from [13], which is very long with large height but small slope. In this paper, the terrain profile is compounded with a Gaussian correlated random roughness with rms height of 2 cm and correlation length of 6 cm as shown in Fig. 1.

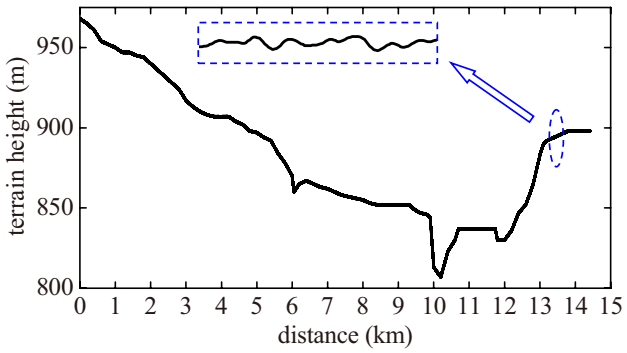

Figure 1. Composite Beiseker N15 profile with Gaussian correlated roughness. rms height $h = 2$ cm, correlation length $l = 6$ cm.

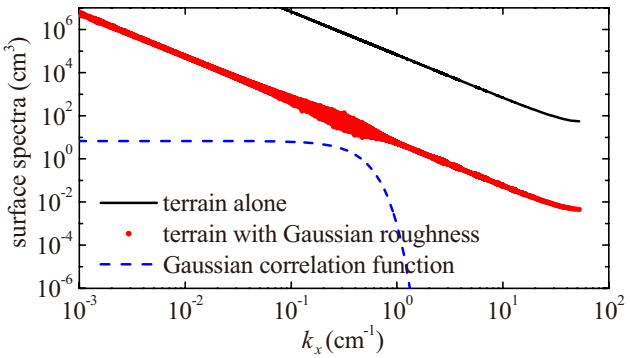

Figure 2. Surface spectra of composite terrain surfaces with Gaussian correlated roughness. Terrain alone, and Gaussian correlated surfaces as reference with $h = 2$ cm and $l = 6$ cm.

To better understand the property of the composite terrain profile with Gaussian correlated roughness, Fig. 2 shows the spectra of the terrain alone, the composite terrain, and the Gaussian correlation function with a 2-cm rms height and a 6-cm correlation length. It is evident that the composite terrain spectrum is approximately log-linear and lies between the single terrain and Gaussian spectra. At high-frequency portions, the composite terrain spectrum has much larger energy than that of Gaussian correlation function. In addition, we also find an interesting phenomenon that the single terrain spectrum can move upwards as the cutoff frequency becomes higher, while the composite terrain spectrum converges stably and is independent of the cutoff frequency.

3. FORMULATIONS OF WAVE PROPAGATION AND SCATTERING PROBLEMS

The formulations and implementation of wave propagation and scattering problems from such composite terrain profile is in order.

3.1. Incident Wave

Consider a circularly polarized wave impinging upon a terrain surface with Gaussian correlated roughness $z = f(x)$. The upper half space above the surface is air with permittivity of ε_0, and the lower dielectric medium is with permittivity of ε_1. The electric field and magnetic field for left-hand/right-

hand circular polarizations are expressed as

$$\bar{E}_{iq} = E_{iv}\hat{v}_i + E_{ih}\hat{h}_i; \quad q = \mathrm{LC}, \mathrm{RC} \tag{1a}$$

$$\eta_0 \bar{H}_{iq} = E_{iv}\hat{h}_i - E_{ih}\hat{v}_i; \quad q = \mathrm{LC}, \mathrm{RC} \tag{1b}$$

where η_0 is the wave impedance in free space, and the polarization vectors are defined as

$$\hat{h}_i = -\sin\varphi_i \hat{x} + \cos\varphi_i \hat{y} \tag{2a}$$

$$\hat{v}_i = -\cos\theta_i \cos\varphi_i \hat{x} - \cos\theta_i \sin\varphi_i \hat{y} - \sin\theta_i \hat{z}. \tag{2b}$$

For this paper, $\varphi_i = 0$, and the polarized components are expressed as

$$E_{ih} = \cos\alpha\psi_{\mathrm{inc}} \exp(-i\beta) \tag{3a}$$

$$E_{iv} = \sin\alpha\psi_{\mathrm{inc}} \tag{3b}$$

where parameters α and β are used to characterize the polarizations with the incident directions given above, $(\alpha, \beta) = (45°, 90°)$ and $(45°, -90°)$, respectively, for left and right hand circular polarizations. The scalar wave ψ_{inc} is tapered the same as [17] for calculating the bistatic scattering coefficients. For wave propagation problem, however, it is expressed by a cylindrical wave of Hankel function

$$\psi_{\mathrm{inc}} = \frac{i}{4} H_0^{(1)}(kR) = \frac{i}{4} H_0^{(1)}\left(k\left|\bar{r} - \bar{r}_a\right|\right) \tag{4}$$

where k denotes the wave number, and $\bar{r}_a$ is the location of the transmitting antenna.

ψ_{inc} of the tapered plane wave is fine for circularly polarized expression (1). When ψ_{inc} becomes cylindrical wave as above, according to Maxwell's theory, only two components of the electromagnetic fields are independent, thus the vertical component E_{iv} can be expressed by E_{ih}

$$E_{iv} = \sin\alpha \frac{i}{4}\left(iH_1^{(1)}(kR)\right) \tag{5}$$

Substituting (4) and (5) into (3b) should have

$$\sin\alpha \frac{i}{4}\left(iH_1^{(1)}(kR)\right) = \sin\alpha \frac{i}{4} H_0^{(1)}(kR) \tag{6}$$

The above formula is verified in Fig. 3, and there is $iH_1^{(1)}(kR) \approx H_0^{(1)}(kR)$ for $kR > 2$ (i.e., $R > 0.32\lambda$). Therefore, cylindrical waves are also reasonable as circularly polarized waves.

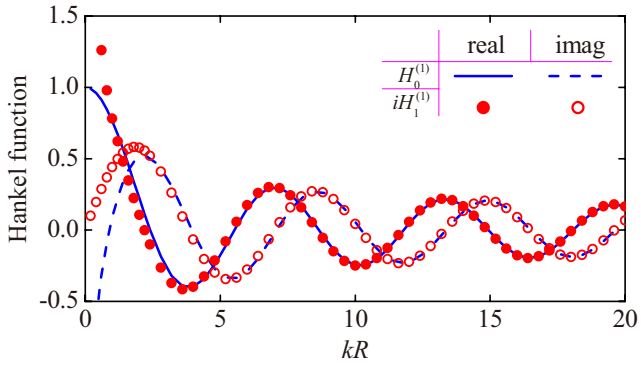

Figure 3. Comparison between cylindrical wave $H_0^{(1)}(kR)$ and $iH_1^{(1)}(kR)$.

3.2. Discretization of Surface Integral Equations

Next, we want to find the scattered field that can be determined from the surface fields, similar to [17], which are unknown to be solved from the surface integral equations in upper and lower regions, respectively, given by:

$$\int_{s'} dx' g_0 \chi_0(x') - \fint_{s'} ds' \psi_0(x') \hat{n}_t' \cdot \nabla_t' g_0 + \frac{1}{2}\psi_0(x) = E_{iy}(x, z) \tag{7a}$$

$$\int_{s'} dx' g_0 \xi_0(x') - \fint_{s'} ds' \phi_0(x') \hat{n}_t' \cdot \nabla_t' g_0 + \frac{1}{2}\phi_0(x) = H_{iy}(x,z) \tag{7b}$$

$$\int_{s'} dx' g_1 \chi_1(x') - \fint_{s'} ds' \psi_1(x') \hat{n}_t' \cdot \nabla_t' g_1 - \frac{1}{2}\psi_1(x) = 0 \tag{7c}$$

$$\int_{s'} dx' g_1 \xi_1(x') - \fint_{s'} ds' \phi_1(x') \hat{n}_t' \cdot \nabla_t' g_1 - \frac{1}{2}\phi_1(x) = 0 \tag{7d}$$

where $\fint$ denotes a principal value of integral, $\nabla_t' = \hat{x}\frac{\partial}{\partial x'} + \hat{z}\frac{\partial}{\partial z'}$, and the Green functions are

$$g_0\left(\bar{r}', \bar{r}\right) = \frac{i}{4} H_0^{(1)}\left(k\left|\bar{r} - \bar{r}'\right|\right) \tag{8a}$$

$$g_1\left(\bar{r}', \bar{r}\right) = \frac{i}{4} H_0^{(1)}\left(k_1\left|\bar{r} - \bar{r}'\right|\right) \tag{8b}$$

E_{iy} and H_{iy} represent the $\hat{y}$ component of incident electric field and magnetic field, respectively. It is easily recognized that the surface fields are the $\hat{y}$ components of surface electric and magnetic fields and their normal derivatives on the surface in upper and lower regions, respectively, given by:

$$\psi_j(x) = E_{jy}(x); \qquad j = 0, 1 \tag{9a}$$

$$\phi_j(x) = H_{jy}(x); \qquad j = 0, 1 \tag{9b}$$

$$\chi_j(x) = \sqrt{1 + f_x^2}\left(\hat{n}_t \cdot \nabla_t E_{jy}(x)\right); \quad j = 0, 1 \tag{9c}$$

$$\xi_j(x) = \sqrt{1 + f_x^2}\left(\hat{n}_t \cdot \nabla_t H_{jy}(x)\right); \quad j = 0, 1 \tag{9d}$$

Substituting the unknown surface fields in (9) into the corresponding integral equations (7), they can be converted into matrix equations. According the following boundary conditions:

$$\psi_1(x) = \psi_0(x) \tag{10a}$$

$$\phi_1(x) = \phi_0(x) \tag{10b}$$

$$\chi_1(x) = \chi_0(x) \tag{10c}$$

$$\xi_1(x) = \rho\xi_0(x) \tag{10d}$$

where $\rho = \varepsilon_1/\varepsilon_0$, then the method of moments is used to discretize the integral equation; the rooftop basic function is selected as the basis function; and the Galerkin's method is used to select the weight function. After being discretized by the method of moments, the matrix equation is

$$\begin{bmatrix} \bar{\bar{A}}_1 & \bar{\bar{B}}_1 & & \\ \bar{\bar{A}}_0 & \bar{\bar{B}}_0 & 0 & \\ & & \bar{\bar{B}}_0 & \bar{\bar{A}}_0 \\ 0 & & \bar{\bar{B}}_1 & \rho\bar{\bar{A}}_1 \end{bmatrix} \begin{bmatrix} \bar{\chi}_0(x) \\ \bar{\psi}_0(x) \\ \eta_0\bar{\phi}_0(x) \\ \eta_0\bar{\xi}_0(x) \end{bmatrix} = \begin{bmatrix} \bar{0} \\ \bar{e} \\ \eta_0\bar{h} \\ \bar{0} \end{bmatrix} \tag{11}$$

where matrix elements and those on the right-hand side can be readily evaluated by [17].

In order to ensure the sampling accuracy, the sampling density is 20 points per wavelength. Let N be the total number of discretization points, and the matrix dimension is $4N \times 4N$. Since the electric and magnetic fields are decoupled, the matrix dimension can be reduced to $2N \times 2N$. In this paper, the inverses of the diagonal blocks are used as a preconditioner to reduce the number of iterations, and the multilevel UV method is applied to accelerate the solution of moment method.

3.3. Polarized Bistatic Scattering Coefficients and Field Strength above Profile

Once the surface electromagnetic fields are solved in (11), the bistatic scattering coefficients for the left-hand and right-hand circular polarizations are computed as [11]

$$\gamma_{pq}(\theta_s) = \frac{\left|\tilde{E}_{sp}^2(\theta_s)\right|}{8k\eta_0 P_{iq}}; \quad \begin{cases} p = \mathrm{L}, \mathrm{R} \\ q = \mathrm{L}, \mathrm{R} \end{cases} \tag{12}$$

where P_{iq} denotes the q-polarized incident power [17], and $\tilde{E}_{sp}$ is given by surface unknowns:

$$\tilde{E}_{s\mathrm{L}}(\theta_s) = \int_{s'} dx' \frac{ik\left(f'_{x'}\sin\theta_s - \cos\theta_s\right)(\eta_0\phi'_0 + i\psi'_0) - (\eta_0\xi'_0 + i\chi'_0)}{\sqrt{2}\exp\left(ik(x'\sin\theta_s + f'\cos\theta_s)\right)} \tag{13a}$$

$$\tilde{E}_{s\mathrm{R}}(\theta_s) = \int_{s'} dx' \frac{ik\left(f'_{x'}\sin\theta_s - \cos\theta_s\right)(\eta_0\phi'_0 - i\psi'_0) - (\eta_0\xi'_0 - i\chi'_0)}{\sqrt{2}\exp\left(ik(x'\sin\theta_s + f'\cos\theta_s)\right)} \tag{13b}$$

$\tilde{E}_{sp}$ with a factor of $\frac{(1+i)\exp(ikr)}{4\sqrt{\pi kr}}$ denoting the p-polarized scattered electric field in the far field point $\bar{r}$ at q-polarized tapered plane wave incidence.

For wave propagation, the scattered field in the near field point $\bar{r}$ such as 1.8-m height above the terrain profile, at q-polarized cylindrical wave incidence, can also be expressed as, respectively, for the left-hand and the right-hand circular polarizations:

$$E_{s\mathrm{L}}(\bar{r}) = \int_{s'} dx' \frac{\eta_0\xi'_0 + i\chi'_0}{\sqrt{2}} g_0\left(x', f'; \bar{r}\right) - \int_{s'} ds' \frac{\eta_0\phi'_0 + i\psi'_0}{\sqrt{2}} \hat{n}'_t \cdot \nabla'_t g_0\left(x', f'; \bar{r}\right) \tag{14a}$$

$$E_{s\mathrm{R}}(\bar{r}) = \int_{s'} dx' \frac{\eta_0\xi'_0 - i\chi'_0}{\sqrt{2}} g_0\left(x', f'; \bar{r}\right) - \int_{s'} ds' \frac{\eta_0\phi'_0 - i\psi'_0}{\sqrt{2}} \hat{n}'_t \cdot \nabla'_t g_0\left(x', f'; \bar{r}\right) \tag{14b}$$

After obtaining the scattered field at a 1.8-m height above the terrain profile, the total field, that is, the electromagnetic receiving signal, can be obtained by superimposing the incident field.

4. NUMERICAL RESULTS AND DISCUSSION

Above-mentioned Fig. 1 shows the composite terrain profile with total length about 14.4 km. The lower half space below the terrain surface is dielectric medium with permittivity of $\varepsilon_1 = 4.0 + 0.5i$. The rms height and correlation length, of the superimposed Gaussian correlated surface are 2 cm and 6 cm, respectively. Simulations are calculated at 1.575 GHz with a right-hand circularly polarized transmitting antenna height of 20 m above the left-most point and a right-hand or left-hand circularly polarized receiving height of 1.8 m above the profile. The field strength is obtained by averaging the total field over 20 realizations, which is calculated at an interval of $\lambda/8$ in the horizontal direction. For the simulations of the scattering coefficient, the incidence angle is fixed at 45°, and the scattering coefficient is also obtained by averaging over 20 realizations.

The BICGstab method is used to solve the impedance matrix equation to obtain surface electric and magnetic fields, and the tolerances of residuals (L^2 norm) are less than 0.8%. The electric and magnetic fields in circular polarizations are decoupled, thus the TE part and TM part in (11) can be solved independently. The total CPUs are 44 hours and 47 hours per realization for surface unknowns of $4N = 6,029,312$, with same memory requirement of about 8 GB, respectively, for propagation problem and bistatic scattering problem.

As seen from Fig. 4, it is evident that the total field for likewise RR polarization is about 40 dB higher than that for counterwise LR polarization, thus transmitting and receiving in likewise configuration is preferred in wireless communication systems, which is completely opposite to the conclusion about GPS signal remote sensing in [9] and [10]. The peak-to-peak signal variations are found to be about half wavelength. Over a distance of a few meters the counterwise polarized signal can vary by 20 dB. These features of the simulation results are in agreement with common sense. We see multipath interferences around 13 km, where the hill slope is facing the transmitter. The results also show deep fading in valley regions at 6 and 10 km; therefore, travelers should go to high places to communicate, and at the same time, the design and site selection of base stations in the communication system should take into account the signal fading in valley.

For reference, bistatic scattering for circular polarizations is also provided as shown in Fig. 5. It can be clearly seen that the bistatic scattering coefficient for likewise RR polarization is 10–20 dB lower than that for counterwise LR polarization, which is expected to be consistent with the GPS signal feature for remote sensing in [9] and [10].

Figure 6 shows the propagation and bistatic scattering over 3 realizations from the composite Brazeau SE18 profile, which is obtained from [16]. The permittivity, overlay roughness, the way that

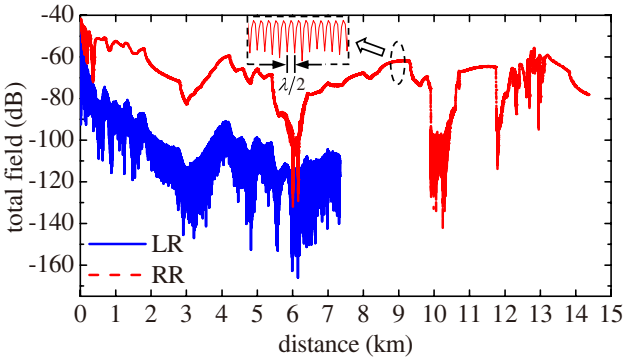

Figure 4. Comparison of total field over 20 realizations at height of 1.8 m above composite Beiseker N15 profile, between likewise and counterwise polarizations.

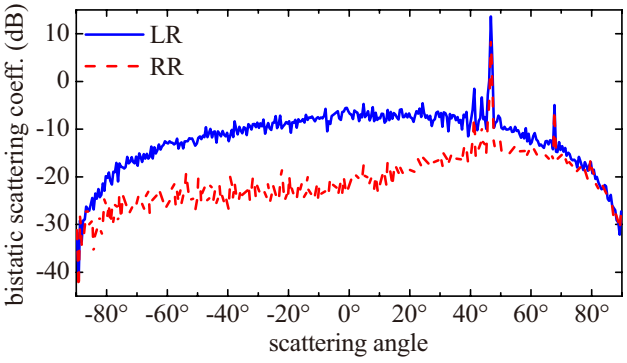

Figure 5. Comparison of bistatic scattering coefficients over 20 realizations between likewise and counterwise polarizations with incident angle $\theta_i = 45°$.

the transmitting and receiving antennas are placed, and other parameters are the same as the former except for the frequency of 900 MHz and the calculating interval of $\lambda/2$. They follow the same rules that RR polarization dominates in propagation, whereas the LR dominates in bistatic scattering. This means that the contradictory phenomena exist for different frequencies and different terrain profiles.

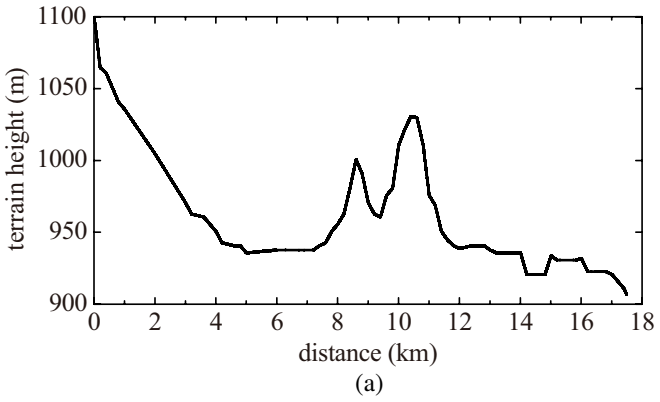

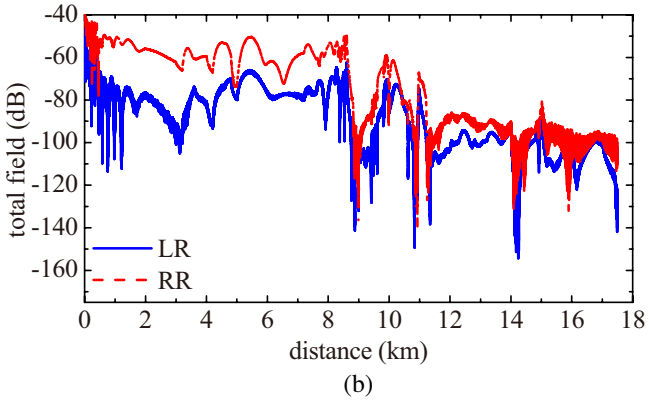

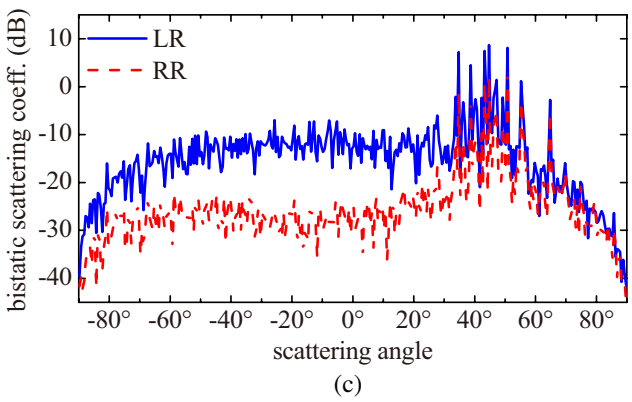

Figure 6. Composite Brazeau SE18 profile, its propagation and bistatic scattering over 3 realizations at frequency of 900 MHz. (a) Composite Brazeau SE18 profile with Gaussian correlated roughness, $h = 2$ cm, $l = 6$ cm. (b) Comparison of total field at height of 1.8 m above composite Brazeau SE18 profile. (c) Comparison of bistatic scattering coefficients with $\theta_i = 45°$.

Comparing the circularly polarized results between propagation and bistatic scattering, it is found that the relative magnitude relationship between likewise and counterwise configurations are completely different, so the circular configuration applied to wireless communication propagation cannot simply copy that in remote sensing. Its physical mechanism will be evidently explained in the following section.

5. PHYSICAL INSIGHT ON ENHANCEMENT OF LIKEWISE OR COUNTERWISE POLARIZATIONS

To fully explain why the field strengths in propagation are larger for the likewise polarization, whereas the bistatic scattering coefficients in remote sensing are larger for counterwise polarization, we investigate the local Fresnel reflection for circular polarization to see which circular polarization is dominant in the two problems, where the Fresnel reflection is an effect of geometric optics. The local Fresnel reflections for circular polarizations can be expressed in terms of the local incident angle θ_ℓ [11]:

$$\left.\begin{matrix} R_{\mathrm{LL}} \\ R_{\mathrm{RR}} \end{matrix}\right\} = \frac{-\sin^2\theta_\ell}{\dfrac{\varepsilon_1+1}{\varepsilon_1-1}\cos\theta_\ell\left(\cos\theta_\ell+\sqrt{\varepsilon_1-\sin^2\theta_\ell}\right)+1} \tag{15a}$$

$$\left.\begin{matrix} R_{\mathrm{RL}} \\ R_{\mathrm{LR}} \end{matrix}\right\} = \frac{\cos\theta_\ell\sqrt{\varepsilon_1-\sin^2\theta_\ell}}{\dfrac{\varepsilon_1+1}{\varepsilon_1-1}\cos\theta_\ell\left(\cos\theta_\ell+\sqrt{\varepsilon_1-\sin^2\theta_\ell}\right)+1} \tag{15b}$$

In Fig. 7, they are plotted as a function of local incident angle θ_ℓ ranging from 0° to 90°. It is obvious that the magnitudes of the counterwise Fresnel coefficients are larger than those of the likewise at smaller local incident angle, and *vice versa*. The former decrease monotonically, while the latter monotonically increase, and they are roughly equivalent around intersection angle $\theta_{\ell\times} = 63°$.

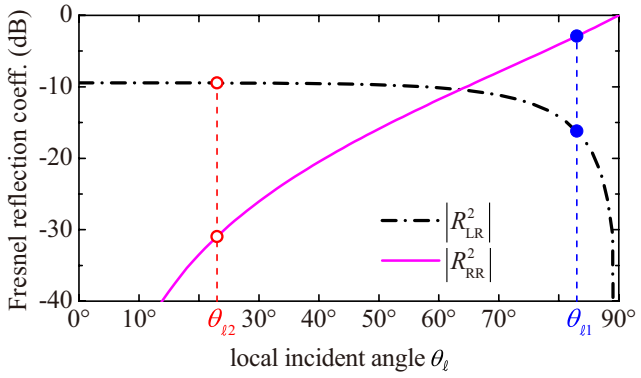

Figure 7. Comparison of Fresnel reflection coefficients between likewise and counterwise polarizations, $\varepsilon_1 = 4.0 + 0.5i$, intersection angle is about $\theta_{\ell\times} = 63°$.

For propagation problem, the height of the left-most transmitting antenna is much less than the length of the terrain profile, so it can be regarded as a grazing incidence. As shown in Fig. 8(a), the local incident angle $\theta_{\ell 1} \to 90° > 63° = \theta_{\ell\times}$, thus, it is shows, in Fig. 7, larger likewise Fresnel reflection. As a result, the likewise field strengths dominate in Fig. 4 and Fig. 6(b). On the other hand, for satellite remote sensing problem, as shown in Fig. 8(b), the local incident angle $\theta_{\ell 2}$ is even smaller than the incident angle θ_i, let alone smaller than the intersection angle $\theta_{\ell\times}$. Thus, it shows, in Fig. 7, larger counterwise Fresnel reflection instead. Correspondingly, the counterwise bistatic scattering coefficient dominates in Fig. 5 and Fig. 6(c).

Completely opposite circular polarization characteristics in wireless communication and remote sensing perhaps offer physical perception to configure likewise polarization for communication, different from counterwise polarization for bistatic sensing.

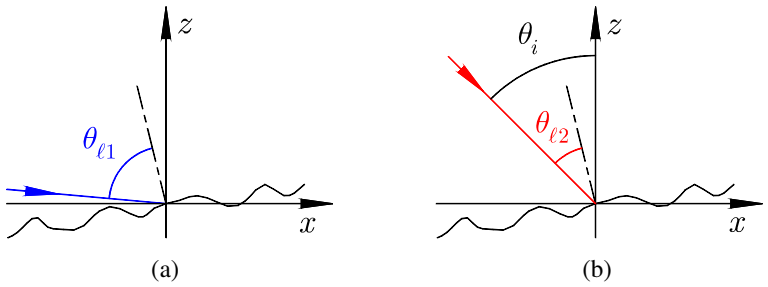

Figure 8. Local incident angles on composite terrain surfaces. (a) For propagation problem, $\theta_{\ell 1} \to 90^\circ > 63^\circ = \theta_{\ell\times}$. (b) For satellite remote sensing problem, $\theta_{\ell 2} < \theta_i = 45^\circ < 63^\circ = \theta_{\ell\times}$.

6. CONCLUSION

The circularly polarized wave propagation over terrain profile is studied by numerical simulation with likewise and counterwise polarizations reception. Results reveal some interesting and abnormal electromagnetic behaviors in that the field strengths of likewise circular polarization can be much larger than the counterwise one, which contradicts the electromagnetic behaviors in remote sensing. Thus it is suggested that for wireless communication over terrain environment by base station signals, both transmitting and receiving polarizations in likewise are adopted.

ACKNOWLEDGMENT

This work was supported in part by the National Natural Science Foundation of China (NSFC) under 41171291, in part by HBUT PhD Startup Funds under 2019057, and in part by National "111 Research Center" Microelectronics and Integrated Circuits.

REFERENCES

1. Ullah, S., C. Ruan, M. S. Sadiq, T. U. Haq, and W. He, "Microstrip system on-chip circular polarized (CP) slotted antenna for THz communication application," *Journal of Electromagnetic Waves and Applications*, Vol. 34, No. 8, 1029–1038, 2020.
2. Tejeswee, S. and S. Verma, "Wide band circularly polarized antenna for (5–7 GHz) WLAN/WiMAX/wireless applications," *Second Int. Conference on Electronics, Communication and Aerospace Technology (ICECA)*, 1290–1294, Coimbatore, 2018.
3. Sharif, A., M. A. Imran, J. Ouyang, Q. H. Abbasi, and Y. Yan, "Circular polarized RFID tag antenna design using characteristic mode analysis," *Int. Workshop on Antenna Technology (iWAT)*, 62–64, Miami, FL, USA, 2019.
4. Genovesi, S., F. Costa, F. A. Dicandia, M. Borgese, and G. Manara, "Orientation-insensitive and normalization-free reading chipless RFID system based on circular polarization interrogation," *IEEE Trans. Antennas Propagat.*, Vol. 68, No. 3, 2370–2378, 2020.
5. Raney, R. K., A. Freeman, and R. L. Jordan, "Improved range ambiguity performance in quad-pol SAR," *IEEE Trans. Geosci. Remote Sens.*, Vol. 50, No. 2, 349–356, 2012.
6. Pincus, P., M. Preiss, A. S. Goh, and D. Gray, "Polarimetric calibration of circularly polarized synthetic aperture radar data," *IEEE Trans. Geosci. Remote Sens.*, Vol. 55, No. 12, 6824–6839, 2017.
7. Yang, P.-J., L.-X. Guo, and Q. Wang, "Circularly polarized wave scattering from two-dimensional dielectric rough sea surface," *Progress In Electromagnetics Research M*, Vol. 44, 119–126, 2015.
8. Yang, P.-J., R. Wu, X. Ren, Y. Zhang, and Y. Zhao, "Doppler spectrum of scattered wave from two-dimensional time-varying nonlinear sea surfaces under right-hand circularly polarized wave incidence," *Progress In Electromagnetics Research B*, Vol. 84, 61–77, 2019.

9. Zavorotny, V. U. and A. G. Voronovich, "Scattering of GPS signals from the ocean with wind remote sensing application," *IEEE Trans. Geosci. Remote Sens.*, Vol. 38, No. 2, 951–964, 2000.
10. Zavorotny, V. U. and A. G. Voronovich, "Bistatic radar scattering from an ocean surface in the small-slope approximation," *Proc. IEEE Int. Geosci. Remote Sens. Symp.*, Vol. 5, 2419–2421, Piscataway, NJ, USA, 1999.
11. Xu, P. and K. S. Chen, "Circularly polarized bistatic scattering from Sastrugi snow surfaces," *IEEE Geosci. Remote Sens. Lett.*, Vol. 14, No. 8, 1398–1402, 2017.
12. Xu, P. and L. Tsang, "Propagation over terrain and urban environment using the multilevel UV method and a hybrid UV/SDFMM method," *IEEE Antennas Wireless Propagat. Lett.*, Vol. 3, 336–339, 2004.
13. Johnson, J. T., R. T. Shin, J. C. Edison, L. Tsang, and J. A. Kong, "A method of moments model for VHF propagation," *IEEE Trans. Antennas Propagat.*, Vol. 45, No. 1, 115–125, 1997.
14. Hviid, J. T., J. B. Andersen, J. Toftgard, and J. Bojer, "Terrain-based propagation model for rural area — An integral equation approach," *IEEE Trans. Antennas Propagat.*, Vol. 43, No. 1, 41–46, 1995.
15. Brennan, C. and P. J. Cullen, "Application of the fast far-field approximation to the computation of UHF pathloss over irregular terrain," *IEEE Trans. Antennas Propagat.*, Vol. 46, No. 6, 881–890, 1998.
16. Ayasli, S., "SEKE: A computer model for low altitude radar propagation over irregular terrain," *IEEE Trans. Antennas Propagat.*, Vol. 34, No. 8, 1013–1023, 1986.
17. Xu, P., K. S. Chen, Y. Liu, J. C. Shi, C. Peng, R. Jiang, and J. Zeng, "Full-wave simulation and analysis of bistatic scattering and polarimetric emissions from double-layered sastrugi surfaces," *IEEE Trans. Geosci. Remote Sens.*, Vol. 55, No. 1, 292–307, 2017.
18. Tsang, L., D. Chen, P. Xu, Q. Li, and V. Jandhyala, "Wave scattering with the UV multilevel partitioning method: 1. Two-dimensional problem of perfect electric conductor surface scattering," *Radio Sci.*, Vol. 39, No. 5, RS5010, 2004.